American Journal of Biological and Environmental Statistics
2025, Vol. 11, No. 3, pp. 42-56
https://doi.org/10.11648/j.ajbes.20251103.11

Research Article

Visual Interpretations of Aqueous Geochemical Data Obtained Around Selected Solid Waste Dumpsites in Abuja, North Central Nigeria

Owolabi Joseph Ayodele, Arogundade Johnson Temitope*, Omali Aurelius Ojoina

Department of Earth Sciences, Faculty of Natural Sciences, Prince Abubakar Audu University, Anyigba, Nigeria

Abstract

The visual interpretation of water samples obtained around some selected dumpsites in federal capital territory, Abuja was done. The interpretation was done in order to ascertain the sources/evolution and the fate of the dissolved constituent of the water samples. The study was necessitated by the fact that the visual interpretation of the aqueous geochemical will reveal the process(s) that predominantly influence the water chemistry. The water samples obtained around these dumpsites were analyzed geochemically in a quality assured laboratory. The geochemical data obtained from the geochemical analyses were interpreted using visual procedures like Piper, Chadha, Gibbs, Schoeller, H-FED and Gaillardet diagram. More than 85% of the water samples are confined to Calcium-bicarbonate field (Ca-HCO_3) and Calcium-Sodium- bicarbonate field ((Ca-Na-HCO_3). The result suggests that there is a clear contribution from the weathering of surrounding basement rocks with the weak acids in the water samples exceeding the strong acids. It was also deduced that water rock interactions is the dominant process that govern the composition of the water samples. This study was conducted to provide a comprehensive visual interpretation of the hydro-geochemical characteristics of water samples collected in the vicinity of selected dumpsites within the Federal Capital Territory, Abuja. The primary objective was to ascertain the sources, evolution, and fate of the water's dissolved constituents, thereby identifying the dominant processes influencing its overall chemistry. The research was initiated based on the critical need to understand how localized anthropogenic activities, such as waste disposal, interact with the underlying geology to affect groundwater quality in a rapidly urbanizing environment. Following a rigorous, quality-assured geochemical analysis in a certified laboratory, the data were subjected to a suite of established visual interpretation methods. The analytical data, encompassing a wide range of major ions, were plotted on several hydro-geochemical diagrams, including Piper, Chadha, Gibbs, Schoeller, HFE-D, and Gaillardet. These graphical tools collectively provided a multi-faceted perspective on the water's hydro-chemical facies and its evolutionary path. The collective findings from these diagrams were highly consistent. Over 85% of the water samples were classified within the Calcium-bicarbonate (Ca-HCO_3) and Calcium-Sodium-bicarbonate (Ca-Na-HCO_3) fields. This hydro-chemical signature unequivocally points to water-rock interaction as the primary process governing the composition of the groundwater. The results suggest a clear and substantial contribution from the chemical weathering of the surrounding basement rocks. Furthermore, the predominance of bicarbonate as a major anion indicates that weak acids are significantly more prevalent than strong acids in the water samples. These findings underscore that while dumpsites remain a potential source of localized contamination, the overarching hydro-chemical signature and compositional evolution of the groundwater in the study area are fundamentally controlled by natural geological processes.

*Corresponding author: arogundadejt@ksu.edu.ng (Arogundade Johnson Temitope)

Received: 8 October 2024; **Accepted:** 28 October 2024; **Published:** 26 August 2025

Keywords

Dumpsites, Visual Interpretation, Water Samples, Abuja, Weathering

1. Introduction

The distinctive chemical properties of water which are the result of the geologic and hydrologic processes and have affected the water chemistry are referred to as hydro-chemical facies. The relative concentrations of major ions and other dissolved components in water samples are used to categorize different hydro-chemical facies. To better understand surface and subsurface hydrologic systems, graphical methods (Piper diagram, Gibbs diagram, HFE-D diagram, Schoeller diagram etc.) can be used for the visualization, classification, and interpretation of aqueous geochemical data [1].

Aqueous geochemical data is made up of different physical and chemical parameters that are influenced by anthropogenic activities and natural processes. These parameters work together to create a variety of hydro-chemical facies, or water types, that change over time and space. To better understand the spatio-temporal evolution of the constituent of surface and groundwater, water-rock interaction, seawater intrusion and mixing of water in the hydrogeologic systems, graphical methods (Piper diagram, Gibbs diagram, Stiff diagram, Schoeller diagram and Chadha diagram) have been extensively used to visualize aqueous geochemical data and classify them into various hydrochemical facies [2-5].

Many python programming libraries have been used in the past for scientific analysis and interpretations. For example, Python libraries like Scipy, Pandas, Numpy, Matplotlib, Pandas, Flopy, Pasta and more recently Wqchartpy have been used for scientific and hydro-geochemical analysis [6-11]. WqchartPy is an open-source Python library that can be used to generate all the geochemical diagrams that using lines of codes. To facilitate interpretation of spatial distribution of leachate in solid waste dumpsites and evolution of groundwater geo- chemistry with respect to groundwater flow dynamics and sample locations in aquifers and geology settings, geochemical diagrams like Piper have proven to be highly useful [12]. Therefore, the aim of this research is to use some graphical methods generated through Wqchartpy to determine the evolution of dissolved constituents of the sampled water with respect to leachate flow from the investigated dumpsites.

2. Materials and Methods

2.1. Site Description

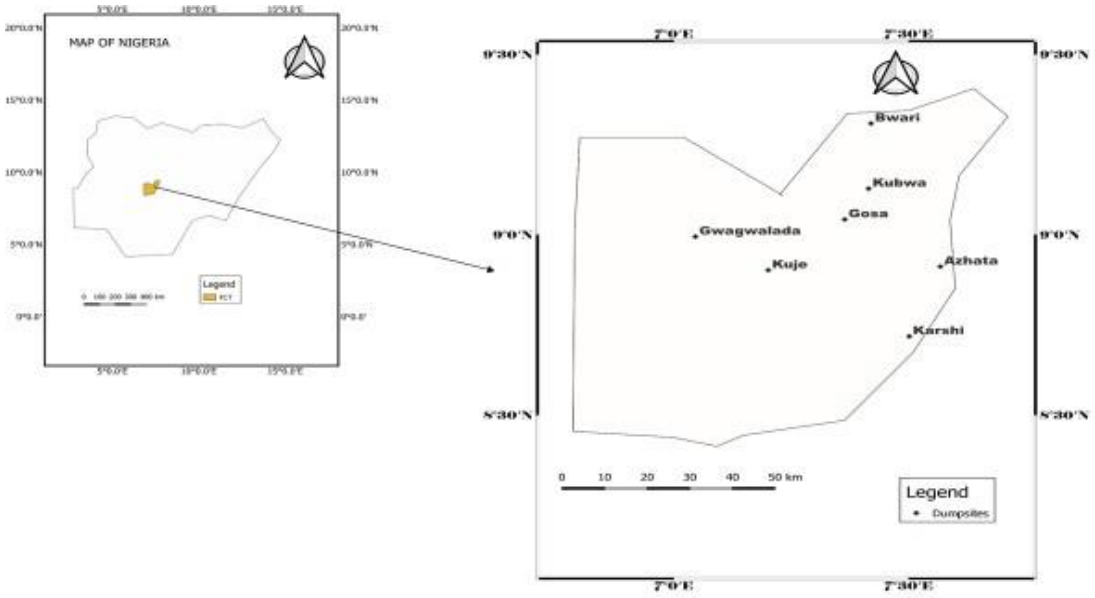

Figure 1. *Map of the study area showing the dumpsites (source: This work).*

The study area is located at the geographical center of Nigeria as shown in figure 1 [13]. It has an estimated population of 6 million people of which 900,000 live and work within the municipality [14, 15]. The study area covers part of FCT Abuja and falls within Latitudes N8°10' and N9°45' and Longitudes E6°30' and E7°45'E, with an approximate area of 120km^2. The Federal Capital Territory of Nigeria has six (6) local councils, which are: Abuja Municipal, Abaji, Bwari, Gwagwalada, Kuje and Kwali [16].

2.2. Geology of the Study Area

The area is underlain by Basement Complex, belonging to Precambrian to Lower Palaezoic on the time scale. The prevalent rocks include igneous rocks of Precambrian age and high grade metarmorphic rocks [17]. It consists mainly of Granite Gneiss, Schist and Migmatite (Figure 2). Groundwater occurrence in this area is controlled by geologic features such as depth of weathering (thickness and continuity of the regolith) and the intensity of fracturing.

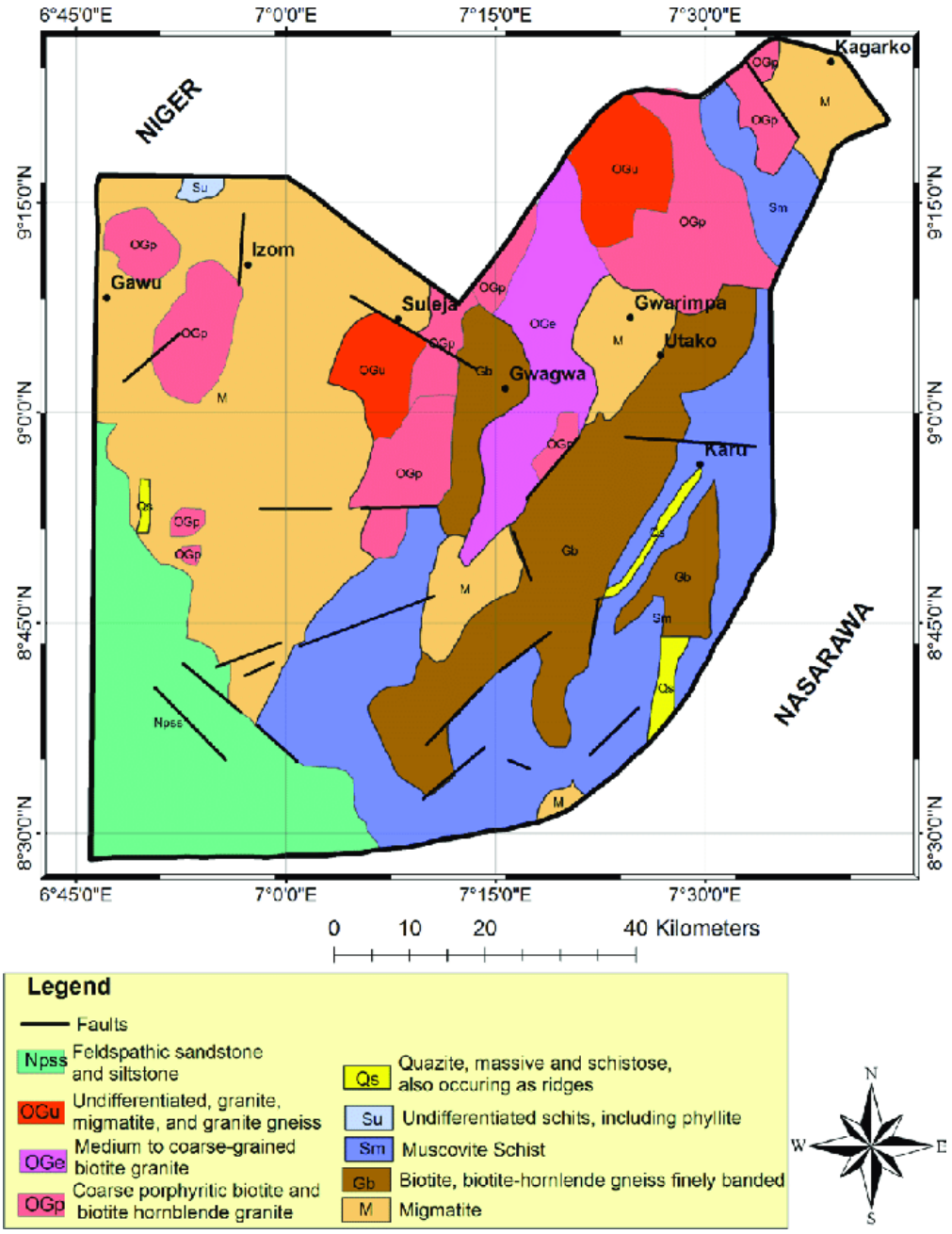

Figure 2. *Geological Map of the study area.*

2.3. Water Sampling and Analytical Method

A total of twenty seven (27) of both surface and groundwater samples were collected directly using 100 ml polythene bottles. Bottles were soaked in 10% HNO3 for 24 hours and rinsed several times with deionised water, prior to sample collection for trace elements and cations [18, 19]. Bottles were also rinsed with aliquots of the sampled water at the time of collection to avoid carryover of contaminants that may compromise the quality of the results [20]. The groundwater samples were collected from hand-dug wells and water boreholes in the vicinity of the study area. Upon arrival at the laboratory, samples were stored in the refrigerator until the day of the analysis. This was done to preserve the integrity of the samples All samples were filtered (using 0.45 µm pore size membrane) and analysed for dissolved trace elements, including cadmium, arsenic, lead, copper, zinc, and nickel, on a Thermo ICAP-RQ inductivity coupled plasma mass spectrometer at the University of Nebraska Water Sciences Laboratory (Lincoln, Nebraska USA). Reagent blanks, laboratory duplicates, and fortified blanks were prepared and used to monitor quality of laboratory measurements. Instrument detection limits are listed with analytical results.

Samples were subjected to microwave assisted acid digestion before they were analysed using ICP-MS. Microwave extraction is designed to mimic extraction using convectional heating with nitric acid (HNO3) or alternatively nitric acid and hydrochloric acid (HCL).

2.4. Quality Assurance

To verify the accuracy of the measurement in this study, standard reference solutions (spiked solutions) with known concentrations of the heavy metals were used as control samples. For the measurements of heavy metals by ICP-MS, certified reference materials (CRMs) and standard reference solutions with known concentrations of elements were recognized as an essential tool for ensuring the quality and establishing the accuracy of the results [21].

Two types of Blanks that were used for the analysis include calibration Blank and rinse Blank. The calibration Blank was used to establish the calibration curve while the rinse Blank was used to flush the system between samples and standards. The sample preparation procedures that were used for samples was also used for the Blanks. All reagents used were of analytical grade. The reliability and reproducibility of the measurements were ensured by calibrating the instruments used and procedural blanks determined.

2.5. The Piper Trilinear Diagram

The Piper trilinear diagram, which plots the concentrations of cations and anions as percentages of the total dissolved solids (TDS) in the water sample, is the most widely used classification scheme for hydrochemical facies [22]. Four quadrants of the diagram represent various hydrochemical facies.

1) Ca-Mg-HCO_3: This facies is characterized by high concentrations of calcium (Ca^{2+}), magnesium (Mg^{2+}) and bicarbonate (HCO^{3-}) ions. This is associated with carbonate rocks such as limestone and dolomite.
2) Na-Cl: This facies is characterized by high concentrations of sodium (Na^{+}) and chloride (Cl-) ions. This is associated with marine and evaporite environments.
3) Na-HCO_3: This facies is characterized by high concentrations of sodium (Na^{+}) and bicarbonate (HCO_3^{-}) ions. This is associated with weathered and altered volcanic rocks.
4) Ca-SO_4: This facies is characterized by high concentrations of calcium (Ca^{2+}) and sulfate (SO_4^{2-}) ions. This is associated with gypsum and anhydrite deposits.
5) Ca-HCO_3: This facies is characterized by high concentrations of calcium (Ca^{2+}) and bicarbonate (HCO_3^{-}) ions, and is associated with carbonate rocks such as limestone and dolomite.
6) Na-Cl: This facies is characterized by high concentrations of sodium (Na^{+}) and chloride (Cl^{-}) ions, and is associated with marine and evaporite environments.
7) Ca-SO_4: This facies is characterized by high concentrations of calcium (Ca^{2+}) and sulfate (SO_4^{2-}) ions, and is associated with gypsum and anhydrite deposits.
8) Mg-Cl: This facies is characterized by high concentrations of magnesium (Mg^{2+}) and chloride (Cl^{-}) ions, and is associated with marine and evaporite environments.
9) Na-HCO_3: This facies is characterized by high concentrations of sodium (Na^{+}) and bicarbonate (HCO^{3-}) ions, and is associated with weathered and altered volcanic rocks.
10) Mixed: This facies is characterized by mixed ion composition and can result from multiple hydrological and geological processes.

2.6. Chadha Diagram

The relationship between two variables, X and Y, in which X is the independent variable and Y is the dependent variable, is graphically depicted in the Chadha diagram. A new diagrammatic method for analyzing the relationship between two variables was first presented by S.P. Chadha in his 1968 paper titled "A New Diagrammatic Method" [23].

The independent variable is represented by the X-axis on the Chadha diagram, while the dependent variable is represented by the Y-axis. The diagram's points each stand for a distinct pairing of X and Y values. A positive relationship between X and Y is represented in the upper-right quadrant of the diagram, a negative relationship is represented in the lower-left quadrant, a non-linear relationship is represented in the upper-left quadrant, and a positive relationship is represented in the lower-right quadrant.

The Chadha diagram can also be used to come up with theories regarding how X and Y relate to one another. For instance, it may indicate a positive linear relationship between X and Y if the majority of the points on the diagram are located in the upper-right quadrant (Chadha, 1968).

The Chadha diagram, in general, is a helpful tool for examining the relationship between two variables, especially when patterns in the data may not be immediately obvious. It is a well-liked tool in many research fields due to its simplicity and clear graphical representation (Chadha, 1968).

2.7. Gaillardet Diagram

This diagram was developed by Gaillardet to investigate types of water-rock interactions for surface water geochemistry [24]. The diagram was designed with the understanding that evaporite dissolution, silicate weathering, and carbonate dissolution control water-rock interactions. The influence of these processes is also clear on two scatter plots. One has the molar ratio of Ca^{2+}/Na+ on the x axis and the molar ratio of HCO_3^- /Na+ on the y axis. In the other plot, HCO_3^- /Na+ is replaced by Mg^{2+}/Na+ on the y axis. The x and y axes are both logarithmic.

2.8. Schoeller Diagram

Schoeller diagram was developed by Schoeller in 1962 as a diagram that can be used to visualize geochemical compositions of multiple water samples in one plot [25]. It is in form of a semi-logarithmic graph whose x axis is of arithmetic scale and it is used for the names of major anions and cations like Mg^{2+}, Ca^{2+}, Na^+, Cl^-, SO_4^{2-}, and HCO_3^- and y axis is in the logarithm scale to plot the milli-equivalent concentrations of these ions. Each sample has its own line in the Schoeller diagram to show not only the absolute parameter values of each sample but also the concentration differences among different samples.

2.9. HFE-D Diagram

HFE-D is an acronym for hydro-geochemical facies evolution diagram. It is a multi-rectangular diagram developed to investigate sea water intrusion and freshening processes [26]. By considering the milli-equivalent percentages of four major cations (Ca^{2+}, Mg^{2+}, Na+, and K^+) and four major anions (SO_4^{2-}, Cl^-, CO_3^{2-}, and HCO_3^-) and their relationships, HFE-D has a total of 16 hydro chemical facies. A conservative mixing line is established between sea water and fresh water on the diagram and any sample that fall above and below the mixing line are likely affected by freshening and intrusion processes, respectively [27, 28]. Understanding the hydro-geochemical processes that regulate the chemistry of water in various environments, including aquifers, surface water bodies, and geothermal systems, can be aided by using the HFE-D diagram. It is based on the relative dominance of major ions in water samples.

2.10. Gibbs Diagram

Gibbs diagram was developed by Gibbs in 1970. It is a diagram designed to study the processes governing the evolution of chemical composition of surface and groundwater based on a large number of water samples [29]. The three major governing processes are precipitation, water-rock interaction, and evaporation. The influence of these processes is clear on two scatter plots. One has molar ratios of Na^+/ $Na^+ + Ca^{2+}$ on the x axis and TDS on the y axis at the logarithmic scale. In the other plot, Na^+/ $Na^+ + Ca^{2+}$ is replaced by Cl^-/ $Cl^- + HCO_3^-$. Water quality data of rivers and lakes dominated by water-rock interactions typically have higher Ca^{2+} and HCO_3^- concentrations than Na+ and Cl- concentrations, and are thus plotted in the middle part of the boomerang. Water samples from oceans commonly have higher Na+, Cl-, and TDS concentrations due to evaporation, and are thus plotted closely to the upper right of the boomerang. Rain water samples have the lowest TDS, and are thus plotted to the lower right of the boomerang.

2.11. Durov Diagram

Durov diagram was developed by Durov in (1948). It is an alternative to the Piper diagram as it also involve plotting of the percentages of major cations and anions in milli-equivalents on two separate triangular panels [30]. The sample points are projected to a square grid at the base of the two triangles. The main purpose of Durov diagram is to cluster data points indicating the samples with similar chemistry as well as to reveal a useful relationship and properties for a large sample group. The Durov Diagram also includes two additional panels for pH and total dissolved solids (TDS), to understand the water chemistry.

3. Results and Discussion

Table 1. *Hydro-geochenical results.*

Sample	Label	EC	TDS	HCO_3	Cl	pH	PO_4	SO_4	Na	K	Mg	Ca
BWw1	Bwari	134.00	254	506	56.2	6.93	0.045	47.2	64.7	10.2	35.4	56.2

Sample	Label	EC	TDS	HCO_3	Cl	pH	PO_4	SO_4	Na	K	Mg	Ca
BWw2	Bwari	127.00	224	368	36.1	6.69	0	2.41	22.2	7.11	5.09	20.6
BWw3	Bwari	11.00	270	414	56.4	6.49	0.015	47.1	38.4	10	35.8	51.6
BWw4	Bwari	91.00	208	311	36.3	6.57	1.54	3.57	38.2	15.2	5.08	35.4
GWw1	Gwagwalada	121.00	320	207	122	6.39	0.028	30.2	50.4	34.9	17.9	34.4
GWw2	Gwagwalada	162.00	209	299	117	6.84	0.034	41.1	54	11.5	29.1	76.7
GWw3	Gwagwalada	117.00	245	322	55.8	6.47	0.015	47.3	63.2	10.2	29.2	54.5
GWw4	Gwagwalada	97.00	234	311	46.7	6.70	0.014	30.5	50.1	13.4	25	46.5
KWw1	Kubwa	165.00	243	219	0.87	6.35	0.063	0.69	12	2.22	2.63	26.7
KWw2	Kubwa	198.00	309	299	33.2	6.43	0.03	33.5	21.7	5.14	9.61	58.9
KWw3	Kubwa	113.00	219	265	21.8	6.76	0.017	1.52	25.6	32.8	15.9	46.4
KWw4	Kubwa	87.00	323	368	54.7	6.69	0.009	53.4	62.9	8.98	32.3	52.5
KWw5	Kubwa	134.00	233	368	55.8	6.69	0.016	46.6	65.1	9.51	33.6	57.5
KRSw1	Karshi	187.00	183	173	18	6.39	0.008	9.58	23.3	54.3	13.3	31.2
KRSw2	Karshi	111.00	167	417	86.3	6.93	0.071	38.3	43.5	11.4	44	51.3
KRSw3	Karshi	142.00	320	342	43.1	6.69	0.67	17.2	43.9	8.5	7.48	67.9
KRSw4	Karshi	78.67	200	321	48.4	6.49	0.015	47.1	38.4	10	35.8	51.6
GOw1	Gosa	162.00	235	299	45.4	6.84	0.051	40.9	61	8.18	34.7	62.8
GOw2	Gosa	168.00	304	306	41.7	6.47	0.047	34.3	48.4	12.4	30.1	51.1
GOw3	Gosa	123.00	243	216	15.9	6.70	0.045	37.8	62.4	11.4	36	38.9
GOw4	Gosa	125.00	236	426	45.8	6.93	0.076	53.8	50	9.8	31.7	46.6
AZHw1	Azhata	132.00	198	254	40.7	6.69	0.87	4.04	41.6	10.43	16.42	37.8
AZHw2	Azhata	112.00	248	394	36.5	6.49	0.26	14.7	36.8	9.4	26.2	52.1
AZHw3	Azhata	123.00	211	279	33.6	6.57	0.78	28.6	31	12.5	15.21	24.6
KUJw1	Kuje	132.00	174	260	116	6.39	0.167	27.5	44	18.8	14.6	21.5
KUJw2	Kuje	107.00	215	267	58.9	6.84	0.079	37	32	8.65	19.8	24.7
KUJw3	Kuje	131.00	241	308	36.4	6.47	0.56	21.6	33.1	9.6	15.6	18.9

Sample	Label	NO_3 -N	Cu	Cd	As	Zn	Pb	Mn	Ni	Fe	Cr
BWw1	Bwari	6.84	4.31	0.005	0.015	9.85	0.026	0.521	0.0711	0.525	0.062
BWw2	Bwari	1.83	2.08	0.001	0.052	4.66	0.015	0.64	0.043	1.104	0.077
BWw3	Bwari	4.9	2.08	0.008	0.017	8.37	0.013	0.93	0.15	0.433	0.109
BWw4	Bwari	0	1.56	0.0011	0.0178	12.3	0.019	0.739	0.055	0.106	0.0138
GWw1	Gwagwalada	0.349	2.54	0.01	0.051	6.86	0.13	1.037	0.045	0.941	0.096
GWw2	Gwagwalada	6.52	1.15	0	0.007	4.75	0.011	0.899	0.075	0.289	0.0101
GWw3	Gwagwalada	24.6	2.82	0.0013	0.034	8.24	0.018	0.41	0.0374	0.268	0.089
GWw4	Gwagwalada	3.26	1.08	0.0015	0.011	1.65	0.0186	0.744	0.086	0.139	0.019
KWw1	Kubwa	0.132	0.24	0.0016	0.067	4.72	0.011	1.106	0	1.086	0.079
KWw2	Kubwa	0.324	0.64	0.0014	0.019	9.53	0.014	1.02	0.022	1.015	0.098

Sample	Label	NO_3 -N	Cu	Cd	As	Zn	Pb	Mn	Ni	Fe	Cr
KWw3	Kubwa	0	4.46	0	0.025	3.62	0.017	0.238	0.0466	0.522	0.034
KWw4	Kubwa	9.24	0.7	0.0015	0.019	7.06	0.024	0.68	0.0745	0.604	0.017
KWw5	Kubwa	4.5	1.6	0.0016	0.016	5.93	0.042	0.19	0.017	0.278	0.03
KRSw1	Karshi	0.118	1.28	0.001	0.018	9.56	0.0235	0.25	0.024	0.136	0.095
KRSw2	Karshi	8.71	5.62	0.0015	0.022	2.08	0.019	0.712	0.089	0.587	0.0112
KRSw3	Karshi	1.65	2.08	0.001	0.0152	4.66	0.025	0.64	0.043	0.146	0.057
KRSw4	Karshi	4.9	1.98	0.005	0.017	8.37	0.003	0.93	0.015	0.433	0.0109
GOw1	Gosa	10.12	1.56	0.001	0.078	12.3	0.022	0.739	0.0505	0.106	0.038
GOw2	Gosa	37.6	2.54	0.0011	0.011	6.86	0.013	0.77	0.0415	0.941	0.096
GOw3	Gosa	5.07	1.15	0.013	0.007	4.75	0.011	0.899	0.075	0.289	0.015
GOw4	Gosa	10.5	2.82	0.001	0.0134	8.24	0.018	0.459	0.0304	0.255	0.089
AZHw1	Azhata	3.25	1.08	0.003	0.011	16.5	0.0126	0.744	0.086	1.09	0.0109
AZHw2	Azhata	8.19	0.24	0.001	0.015	4.72	0.021	0.646	0	1	0.091
AZHw3	Azhata	0.98	1.56	0.0011	0.0108	12.3	0.009	0.739	0.051	0.106	0.01
KUJw1	Kuje	0.596	2.54	0.0016	0.0191	6.86	0.013	0.437	0.045	0.941	0.096
KUJw2	Kuje	6.52	1.15	0.0013	0.007	4.75	0.018	0.85	0.075	0.289	0.0119
KUJw3	Kuje	11.5	2.82	0.0021	0.034	8.24	0.018	1.01	0.0341	0.21	0.089

3.1. Piper Diagram

The hydro-chemical facies do not only classify water samples but also reveal their sources and evolutions in a complex hydro-geologic environment. Generally, the rectangular piper diagram just like triangular piper diagram classifies the sample points in the diagram into 6 fields. They are Calcium bicarbonate type; Sodium chloride type; Calcium-Magnesium-Chloride type; Calcium- Sodium-bicarbonate-type; Calcium-Chloride type and Sodium bicarbonate type. However, in the present study (Figures 3 and 4) all the samples are confined to Calcium-bicarbonate field (Ca-HCO_3) and Calcium-Sodium-bicarbonate field ((Ca-Na-HCO_3). The result suggests that there is a clear contribution from the weathering of surrounding basement rocks. It can also be deduced from the results that the weak acid in the water samples exceeded the strong acid.

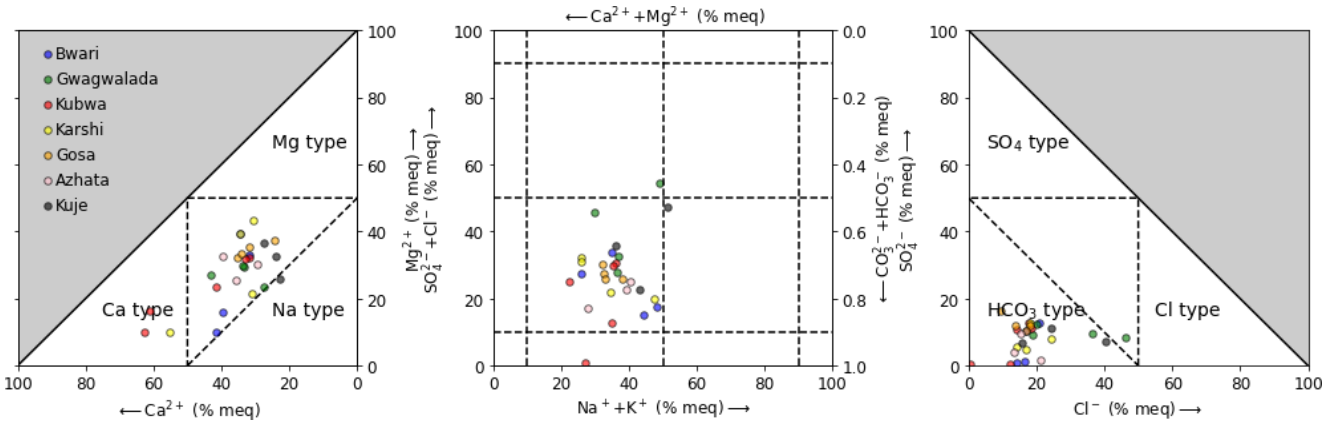

Figure 3. Rectangular Piper diagram for the water samples from the study area.

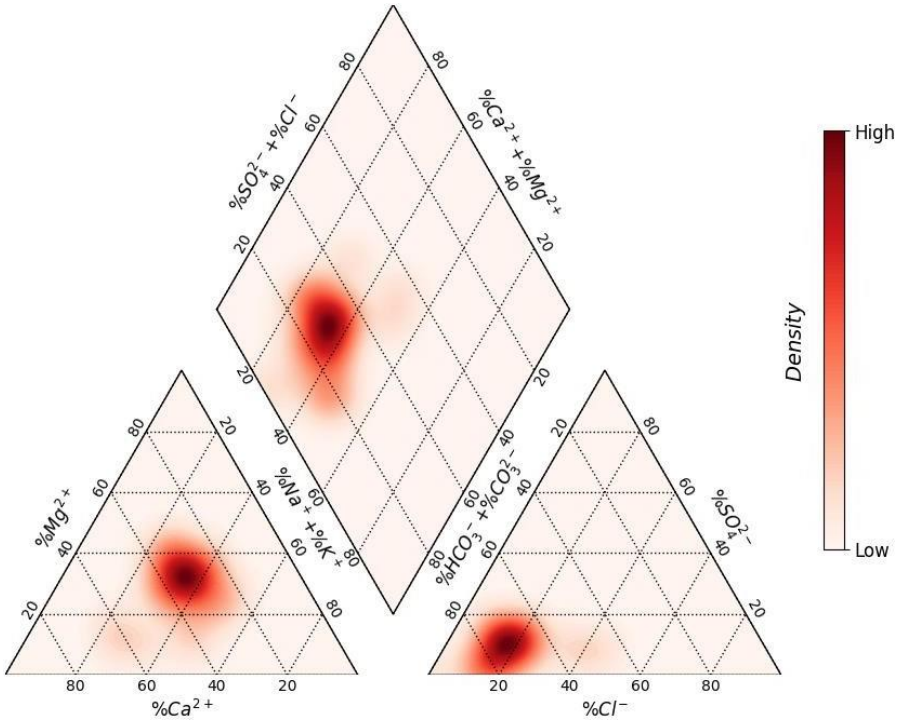

Figure 4. *Coloured piper diagram of the water samples from the study area.*

3.2. Gaillardet Diagram

Water resulting from evaporite dissolution often has higher Na+ concentration than Ca^{2+}, HCO_3^- and Mg^{2+} concentrations, and are thus plotted on the bottom-left corner of the scatter plots. For water resulting from carbonate dissolution are characterized, the concentration of Ca and Mg will be higher if there is dominance of carbonate dissolution. In the present study (Figure 5), all the samples are plotted in the silicate region which mean silicate weathering is the dominant process that governs the water-rock interaction in the study area.

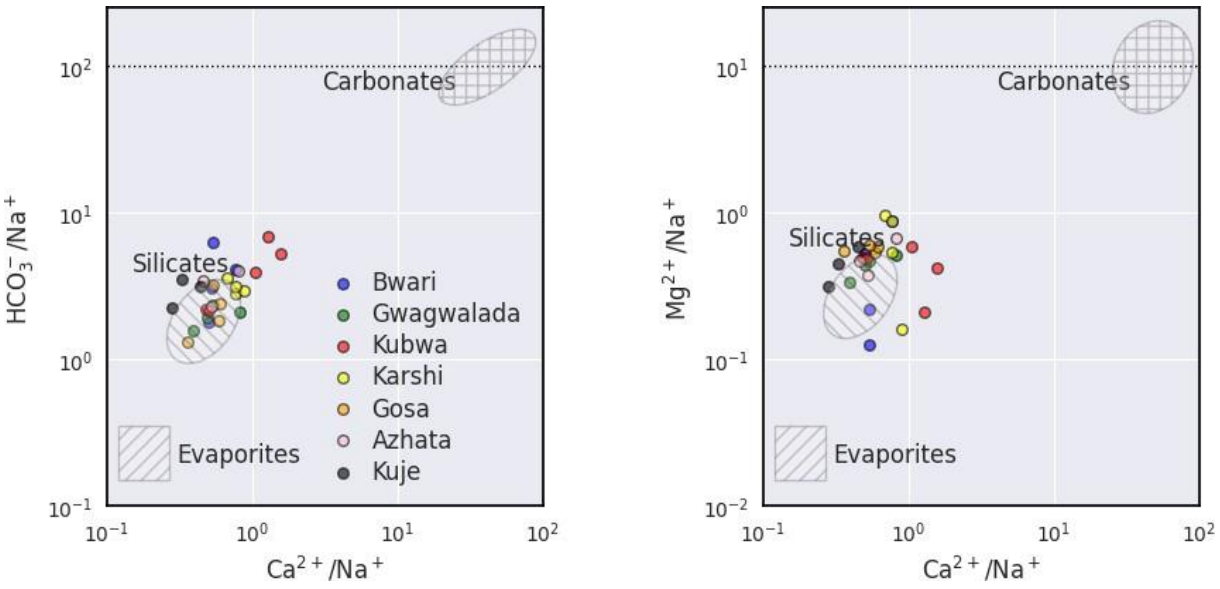

Figure 5. *Gaillardet diagram of water samples from the study area.*

3.3. Schoeller Diagram

The major cations and anions (Ca2+, Mg2+, Na+, K+, Cl-, $SO4^{2-}$and HCO_3^-) of the groundwater samples from the study area were plotted on the Schoeller diagram (Figure 6). The result revealed that Ca2+ and Na+ are the dominant cations while HCO_3^-- is the dominant anion. This mean that the dominant acid in the samples are weak acid and there is simple dissolution and mixing of the ions.

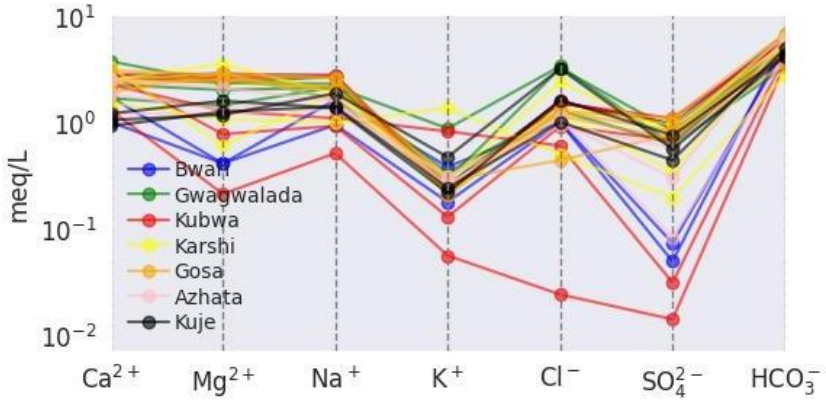

Figure 6. *Schoeller diagram of the groundwater samples from the study area.*

3.4. Durov Diagram

The geochemical evolution of the water samples obtained from the study was assessed using Durov diagram. Just like the result from Piper diagram (Figure 3), 85% of the water samples obtained from the study area are plotted in the mixed field of Ca-Mg-HCO and Ca-Na-HCO_3 (Figure 7).

According to Lloyd and Heathcoat (1985), the result indicate that the water exhibit simple dissolution or mixing.

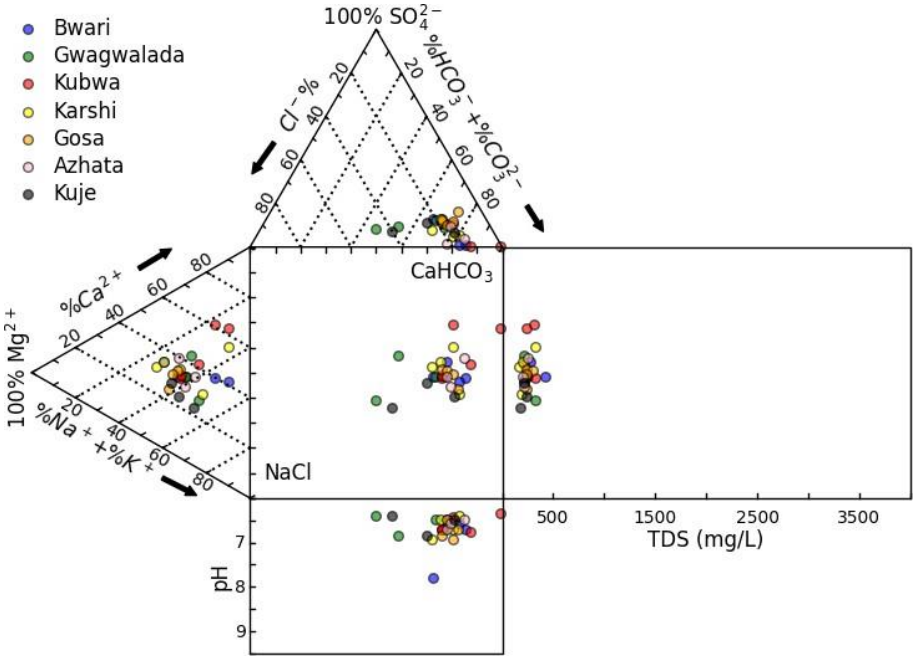

Figure 7. *Durov diagram for water samples from the study area.*

3.5. HFE-D Diagram

In the present study as shown in (Figure 8), 48% each of the whole samples were respectively plotted in field 5 (Mix Na-HCO_3/ $SO4^{2-}$) and field 9 (Mix Ca- HCO_3/ $SO4^{2-}$). The result indicate that the water in the study exhibit simple dissolution or mixing with no salt water intrusion. The water in

the study area exhibit greater percentage of freshening. The surrounding rocks have little influence on the chemistry of the sampled waters.

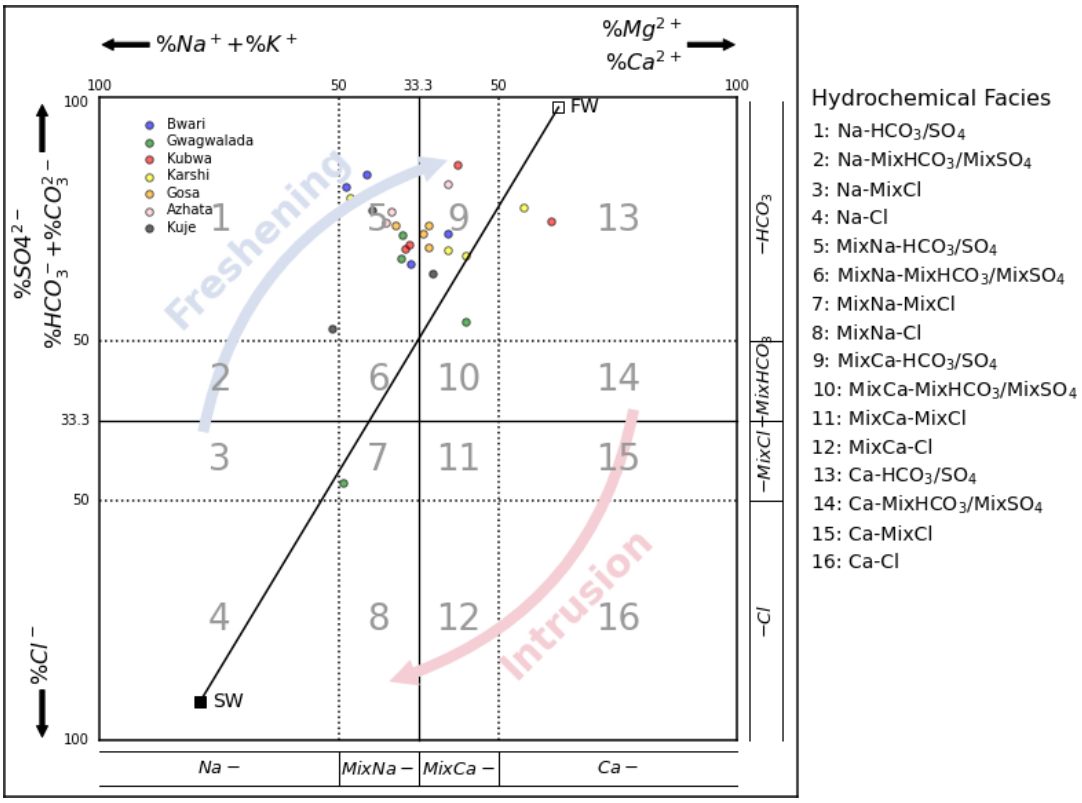

Figure 8. *HFE-D of groundwater samples from the study area.*

3.6. Chadha Diagram

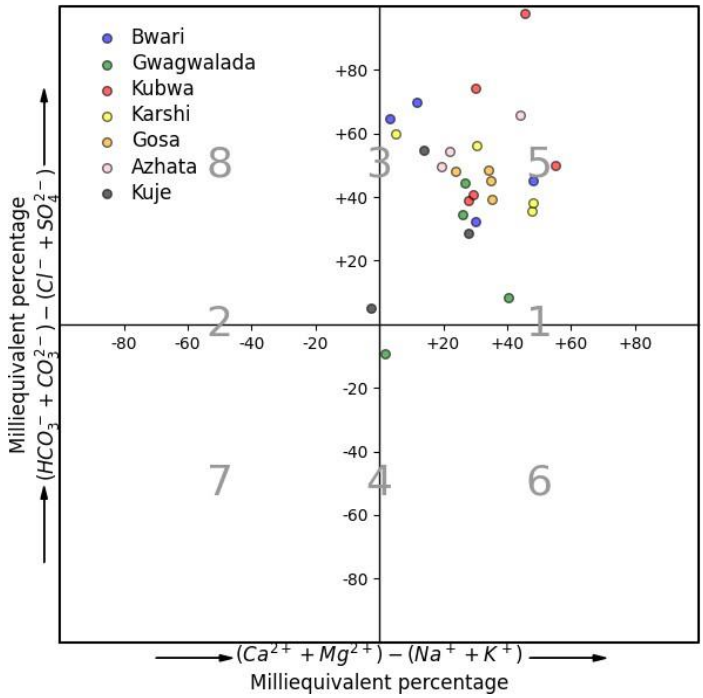

Figure 9. *Chadha diagram of water samples from the study area.*

As shown in Figure 9, 85% of the samples are plotted in the in the Ca-Mg-HCO_3 field while the remaining 15% are plotted in Mix Ca-Na-HCO_3 field. The result indicate that the water in the study area exhibit simple dissolution and mixing. The dominance of Ca-Mg-HCO_3 can also be attributed to the weathering of the surrounding basement rocks.

3.7. Gibbs Diagram

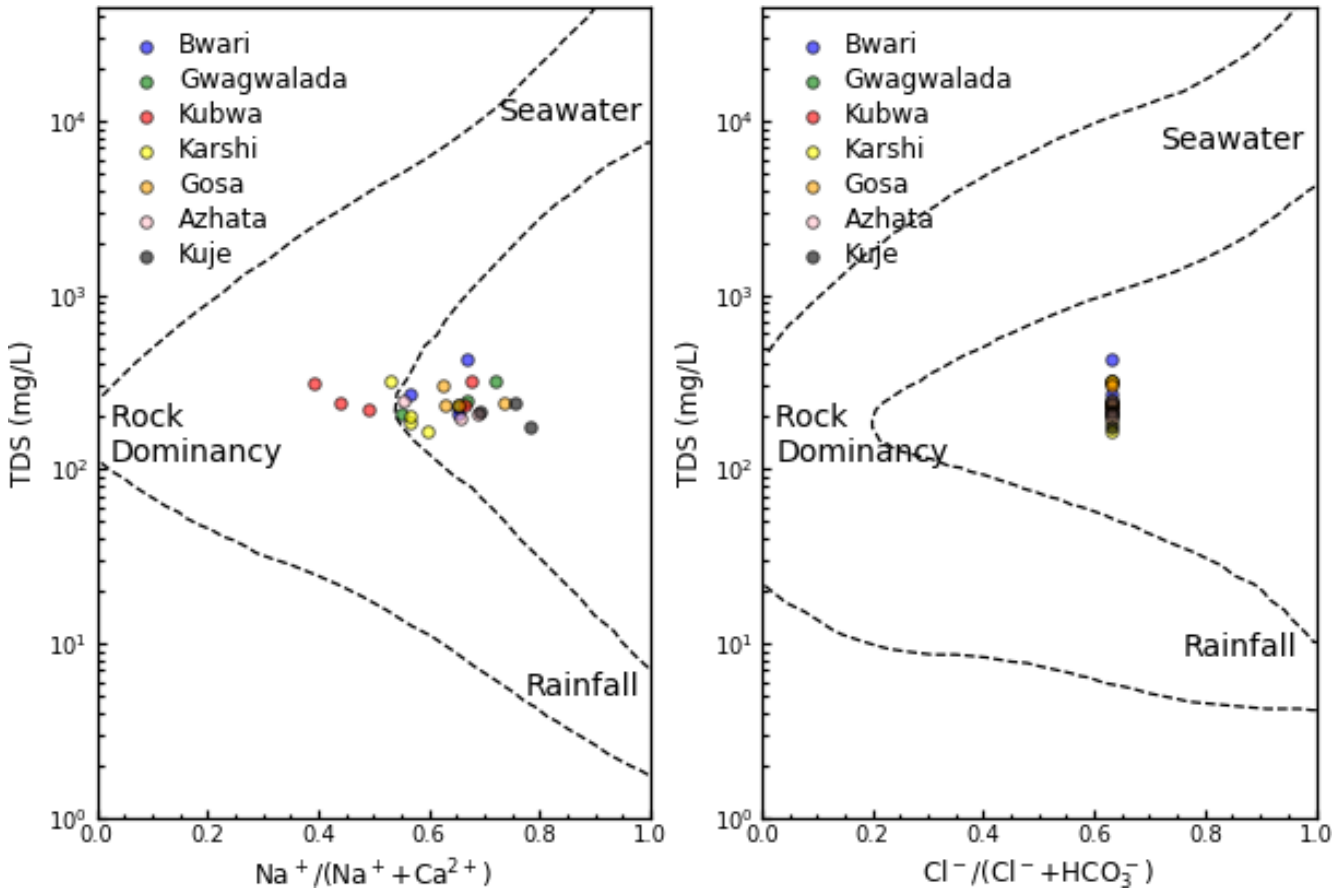

Figure 10. Gibbs diagram of the water samples from the study area.

As shown in Figure 10, all the water samples obtained from the study are plotted in the central part of the boomerang because all the samples have higher Ca^{2+} and HCO_3^- concentrations than Na^+ and Cl^- concentrations. This implies that the water in the study area are dominated by water- rock interaction. The chemical composition of the water samples can be attributed to the weathering of the surrounding basement rocks.

4. Statistical Analysis of the Results

Table 2. Descriptive statistics of the hydro-geochemical results.

	Mean	Median	Mode	STD	Min.	Max.
EC	125.58	125.00	134.00	36.89	11.00	198.00
TDS	239.48	235.00	320.00	43.99	167.00	323.00
HCO^{3-}	315.52	308.00	368.00	75.73	173.00	506.00
Cl^-	50.35	45.40	55.80	29.44	0.87	122.00

	Mean	Median	Mode	STD	Min.	Max.
pH	6.63	6.69	6.69	0.18	6.35	6.93
PO_4^{2-}	0.20	0.05	0.02	0.37	0.00	1.54
SO_4^{2-}	29.54	33.50	47.10	17.22	0.69	53.80
Na^+	42.89	43.50	38.40	14.91	12.00	65.10
K^+	13.57	10.20	10.20	10.73	2.22	54.30
Mg^{2+}	22.87	25.00	35.80	11.65	2.63	44.00
Ca^{2+}	44.40	46.60	51.60	15.39	18.90	76.70
$NO^{3-}N$	6.38	4.90	4.90	8.20	0.00	37.60

Table 3. *Descriptive statistics for the heavy metals in the water samples.*

	Mean	Median	Mode	STD	Min.	Max.
Cu^{2+}	1.988	1.600	2.080	1.275	0.240	5.620
Cd^{2+}	0.003	0.001	0.001	0.003	0.000	0.013
As^{3+}	0.023	0.017	0.011	0.018	0.007	0.078
Zn^{2+}	7.323	6.860	12.300	3.415	1.650	16.500
Pb^{2+}	0.026	0.018	0.013	0.026	0.011	0.130
Mn^{2+}	0.703	0.739	0.739	0.250	0.190	1.106
Ni^{2+}	0.051	0.045	0.075	0.032	0.000	0.150
Fe^{2+}	0.513	0.433	0.106	0.362	0.106	1.104
Cr^{3+}	0.054	0.057	0.096	0.037	0.010	0.109

Table 4. *Pearson r' correlation for the results.*

	EC	*TDS*	HCO^{3-}	Cl	*pH*	PO_4^{3-}	SO_4^{2-}	Na^+	K^+	Mg^{2+}	Ca^{2+}	NO^{3-} N
EC	1											
TDS	0.04	1										
HCO^{3-}	-0.37	0.13	1									
Cl-	-0.13	-0.04	0.11	1								
pH	-0.09	-0.19	0.50	0.12	1							
PO_4^{3-}	-0.10	-0.15	-0.08	-0.17	-0.08	1						
SO_4^{2-}	-0.24	0.22	0.45	0.40	0.32	-0.46	1					
Na^+	-0.15	0.20	0.34	0.41	0.42	-0.16	0.69	1				
K^+	0.15	-0.19	-0.48	0.09	-0.25	-0.08	-0.28	-0.16	1			
Mg^{2+}	-0.34	-0.04	0.48	0.28	0.45	-0.46	0.80	0.70	-0.17	1		
Ca^{2+}	0.06	0.33	0.42	0.19	0.36	-0.23	0.48	0.52	-0.22	0.51	1	
NO^{3-} N	0.08	0.25	0.22	0.02	0.01	-0.21	0.39	0.40	-0.23	0.45	0.25	1

Table 5. Pearson r' correlation for the heavy metals in the water samples.

	Cu^{2+}	Cd^{2+}	As 3+	Zn^{2+}	Pb^{2+}	Mn^{2+}	Ni^{2+}	Fe^{2+}	Cr^{3+}
Cu^{2+}	1.00								
Cd^{2+}	0.01	1.00							
As^{3+}	0.00	-0.03	1.00						
Zn^{2+}	-0.17	0.02	0.05	1.00					
Pb^{2+}	0.11	0.39	0.29	-0.06	1.00				
Mn^{2+}	-0.33	0.38	0.19	0.02	0.07	1.00			
Ni^{2+}	0.21	0.34	-0.29	0.03	-0.07	0.17	1.00		
Fe^{2+}	-0.08	0.06	0.22	-0.05	0.14	0.23	-0.19	1.00	
Cr^{3+}	0.05	0.05	0.28	0.00	0.22	-0.03	-0.28	0.38	1.00

Correlation between the dissolved constituents of water provides clues about their origin and migration. Parameters with high correlation between them indicates the same source and similar transformation and migration processes. As Suresh *et al.* (2011) pointed out, correlation may indicate mutual dependency in addition to migration and other sources. If no correlation is found between elements, it means that the metals are not controlled by a single factor. In this study, a strong correlation was found between all metals except Zn.

5. Conclusion

More than 85% of the water samples are confined to Calcium-bicarbonate field (Ca-HCO_3) and Calcium-Sodium-bicarbonate field (Ca-Na-HCO_3). The result suggests that there is a clear contribution from the weathering of surrounding basement rocks. It can be deduced from the results that the weak acid in the water samples exceed the strong acid. It was also deduced that water rock interactions is the dominant process that govern the composition of the water samples.

Abbreviations

HFE-D Hydro-geochemical Facies Evolution Diagram

Author Contributions

Owolabi Joseph Ayodele: Conceptualization, Data curation, Methodology, Supervision, Writing - original draft, Writing - review & editing

Arogundade Johnson Temitope: Conceptualization, Funding acquisition, Supervision, Visualization, Writing - original draft, Writing - review & editing

Omali Aurelius Ojoina: Conceptualization, Data curation, Funding acquisition, Methodology, Project administration, Supervision, Writing - original draft, Writing - review & editing

Conflicts of Interest

The authors declare no conflicts of interest.

References

[1] Yang J, Liu H & Tang Z, 2022 Visualization of Aqueous Geochemical Data Using Python and WQChartPy, Ground water 60(4) https://doi.org/10.1111/gwat.13185

[2] Pant, R. R., F. Zhang, F. U. Rehman, G. Wang, M. Ye, C. Zeng, and H. Tang. 2018. Spatiotemporal variations of hydrogeochemistry and its controlling factors in the Gandaki River Basin, Central Himalaya Nepal. Science of the Total Environment 622-623: 770-782.

[3] Yang, J., M. Ye, Z. Tang, T. Jiao, X. Song, Y. Pei, and H. Liu. 2020. Using cluster analysis for understanding spatial and temporal patterns and controlling factors of groundwater geochemistry in a regional aquifer. Journal of Hydrology 583: 124594.

[4] Liu, H., J. Yang, M. Ye, S. C. James, Z. Tang, J. Dong, and T. Xing. 2021a. Using t-distributed Stochastic Neighbor Embedding (t-SNE) for cluster analysis and spatial zone delineation of groundwater geochemistry data. Journal of Hydrology 597: 126146.

[5] Liu, H., J. Yang, M. Ye, Z. Tang, J. Dong, and T. Xing. 2021b. Using one-way clustering and co-clustering methods to reveal spatio-temporal patterns and controlling factors of groundwater geochemistry. Journal of Hydrology 603: 127085.

[6] Virtanen, P., Gommers, R., Oliphant, T. E., Haberland, M., Reddy, T., Cournapeau, D., Burovski, E., Peterson, P., Weckesser, W., Bright, J., van der Walt St´efan, J., Brett, M., Wilson, J., Millman, K. J., Mayorov, N., Nelson, A. R. J., Jones, E., Kern, R., Larson, E., Carey, C. J., Polat, ˙I., Feng, Y., Moore, E. W., VanderPlas, J., Laxalde, D., Perktold, J., Cimrman, R., Henriksen, I., Quintero, E. A., Harris, C. R., Archibald, A. M., Ribeiro, A. H., Pedregosa, F., van Mulbregt, P., Vijaykumar, A., Bardelli Alessandro, P., Rothberg, A., Hilboll, A., Kloeckner, A., Scopatz, A., Lee, A., Rokem, A., Woods, C. N., Fulton, C., Masson, C., H¨aggstr¨om, C., Fitzgerald, C., Nicholson David, A., Hagen David, R., Pasechnik Dmitrii, V., Olivetti, E., Martin, E., Wieser, E., Silva, F., Lenders, F., Wilhelm, F., Young, G., Price Gavin, A., Ingold, G.-L., Allen Gregory, E., Lee Gregory, R., Audren, H., Probst, I., Dietrich J¨org, P., Silterra, J., Webber James, T., Slavi˘c, J., Nothman, J., Buchner, J., Kulick, J., Sch¨onberger Johannes, L., de Miranda Cardoso Jos´e, V., Reimer, J., Harrington, J., Rodr´ıguez Juan Luis, C., Nunez-Iglesias, J., Kuczynski, J., Tritz, K., Thoma, M., Newville, M., K¨ummerer, M., Bolingbroke, M., Tartre, M., Pak, M., Smith Nathaniel, J., Nowaczyk, N., Shebanov, N., Pavlyk, O., Brodtkorb Per, A., Lee, P., McGibbon Robert, T., Feldbauer, R., Lewis, S., Tygier, S., Sievert, S., Vigna, S., Peterson, S., More, S., Pudlik, T., Oshima, T., Pingel Thomas, J., Robitaille Thomas, P., Spura, T., Jones Thouis, R., Cera, T., Leslie, T., Zito, T., Krauss, T., Upadhyay, U., Halchenko Yaroslav, O., and V´azquez-Baeza, Y. 2020. SciPy 1.0: fundamental algorithms for scientific computing in Python. Nature Methods 17, no. 3: 261-272 http://dx.doi.org/10.1038/s41592-019-0686-2

[7] McKinney, W. 2010. Data structures for statistical computing in python. In: Proceedings of the 9th Python in Science Conference 445: 56-61.

[8] Harris, C. R., K. J. Millman, S. J. van der Walt, R. Gommers, P. Virtanen, D. Cournapeau, E. Wieser, J. Taylor, S. Berg, N. J. Smith, R. Kern, M. Picus, S. Hoyer, M.. van Kerkwijk, M. Brett, A. Haldane, J. F. Del Rio, M. Wiebe, P. Peterson, P. Gerard-Marchant, K. Sheppard, T. Reddy, W. Weckesser, H. Abbasi, C. Gohlke, and T. E. Oliphant. 2020. Array programming with NumPy. Nature 585, no. 7825: 357-362.

[9] Hunter, J. D. 2007. Matplotlib: A 2D graphics environment. Computing in Science & Engineering 9, no. 3: 90-95.

[10] Bakker, M., V. Post, C. D. Langevin, J. D. Hughes, J. T. White, J. J. Starn, and M. N. Fienen. 2016. Scripting MODFLOW model development using python and FloPy. Ground Water 54, no. 5: 733-739.

[11] Collenteur, R. A., M. Bakker, R. Calj´e, S. A. Klop, and F. Schaars. 2019. Pastas: Open source software for the anal- ysis of groundwater time series. Groundwater 57, no. 6: 877-885.

[12] Peeters, L. 2014. A background color scheme for piper plots to spatially visualize hydrochemical patterns. Ground Water 52, no. 1: 2-6.

[13] Adama, O. (2007) Governing from above: Solid waste management in Nigeria's new capital city of Abuja. Ph.D. Thesis, Stockholm University, Sweden.

[14] NPC. National Population Commission of Nigeria Website (2012). Available www.population.gov.ng

[15] Olanrewaju O and Ilemobade A. (2009) Waste to wealth: A case study of the Ondo State integrated wastes recycling and treatment project. Nigerian, European Journal of Social Sciences. 8(1): 7-16.

[16] Ezeah, C., Roberts, C. L., Watkin, G. D, Philips, P. S. and Odunfa, A. (2009a) Analysis of barriers affecting the adoption of a sustainable municipal solid waste management system in Nigeria. In the proceedings of the 24th International Conference on Solid Waste Technology and Management, 12 - 15 March, 2009. Widener University, Philadelphia, P. A, USA, pp. 1556-1564.

[17] Dada, S. S. (2006). Proterozoic evolution of Nigeria. In: Oshin, O. (ed.). The Basement Complex of Nigeria and its mineral resources. Ibadan, Nigeria, Akin Jinad & Co.

[18] Edet, A. E and Okereke, C. (2003). Contribution to the development of groundwater resources in the Precambrian Oban Massif, south-eastern Nigeria, based on geo-electrical and hydrochemical data. In: J. Krasny, Z. Hrkal & J. Bruthans (Eds.). *Groundwater in fractured rocks* (pp. 249 - 250). Prague, Czech Republic.

[19] Elueze, A. A Ekwere. A. S and Nton M. E (2009) Geoenvironmental assessment of the environs of the Aluminium Smelting Company in Ikot Abasi, south-eastern Nigeria, Journal of Mining and Geology Vol. 45(2) pp. 115-129.

[20] Duce, R. A., Quinn, J. G. Olney, C. E., Poitrowiecz, S. R., Ray, S. J. and Wade, T. L. 1972. Enrichment of heavy metals and organic compounds in the surface micro layer of Narragansett Bay, Rhode Island. Science 176, pp. 161-163.

[21] USEPA. Edition of the Drinking Water Standards and Health Advisories (2012): EPA 822-S-12-001. Washington, DC: Office of Water U.S. Environmental Protection Agency.

[22] Piper, A. M. (1944). A graphic procedure in the geochemical interpretation of water analyses Transactions, American Geophysical Union, 25(6), 914-923.

[23] Chadha, S. P. (1968). A New Diagrammatic Method for Analyzing the Relationship between Two Variables. Journal of the American Statistical Association, 63(324), 758-767.

[24] Gaillardet, J., B. Dupr´e, P. Louvat, and C. J. All`egre. 1999. Global silicate weathering and CO_2 consumption rates deduced from the chemistry of large rivers. Chemical Geology 159, no. 1: 3-30.

[25] Schoeller, H. 1962. Les eaux souterraines. Paris: Masson.

[26] Gimenez-Forcada, E. 2010. Dynamic of sea water interface using hydrochemical facies evolution diagram. Ground Water 48, no. 2: 212-216.

[27] Appelo, C. A. J., and D. Postma. 2005. Geochemistry, Groundwater and Pollution. Great Britain: Taylor and Francis.

[28] Gimenez-Forcada, E., and F. J. Sanchez San Roman. 2015. An excel macro to plot the HFE-diagram to identify Sea water intrusion phases. Ground Water 53, no. 5: 819-824.

[29] Durov, S. A. 1948. Natural waters and graphic representation of their composition. Doklady Akademii Nauk SSSR 59: 87-90.

[30] Gibbs, R. J. 1970. Mechanisms controlling world water chemistry. Science 170, no. 3962: 1088-1090.